

Spatiotemporal evolution and Meteorological triggering conditions of hydrological drought in the Hun River basin, NE China

Shupeng Yue^{1,2}, Fengtian Yang^{1,2}, Xiaodan Sheng³

¹ College of New Energy and Environment, Jilin University, Changchun 130021, China

² MOE Key Laboratory of Groundwater Resources and Environment, Jilin University, Changchun 130021 China

³ Dahuofang Reservoir Authority of Liaoning Province Liability Company, Fushun 11300 China

Correspondence to: Shupeng Yue (yuesp_123@163.com); Fengtian Yang (yangfengtian@jlu.edu.cn)

Abstract. The change of climate and environmental conditions has obviously effecting on the evolution and propagation of drought in river basins. Hun River basin (HRB) is a region seriously troubled by drought in China, so it is particularly urgent to evaluate the evolution of hydrological drought and investigate the threshold of triggering hydrological drought in HRB. In this study, Standardized runoff Index (SRI) was implied to reveal the evolution characteristics of hydrological drought. Meanwhile, based on drought duration and severity identified by the run theory, the copula function with the highest goodness of fit was selected to calculate the return period of hydrological drought. Furthermore, the propagation time from meteorological to hydrological drought were determined by calculating the Pearson correlation coefficients between 1-month SRI and multi-time scale Standardized precipitation index (SPI). Finally, based on the improvement of the drought propagation model, the drought propagation thresholds for triggering different scenarios of hydrological drought and its potential influence factors were investigated. The results show that: (1) hydrological drought showed a slight strengthening trend in the eastern, while presented alternate characteristics of drought and flood in the western and center of the HRB; (2) the western and center of the HRB were vulnerable districts to hydrological drought with longer drought duration and higher severity; (3) the most severe drought with drought duration of 23 months, severity of 28.7, and corresponding return periods that both exceed the thresholds of duration and severity and exceed the threshold of duration or severity were 371 years and 89 years, respectively; (4) the propagation time from meteorological to hydrological drought in the downstream of large reservoir has been significantly prolonged owing to the operation of large reservoir; and (5) the drought propagation threshold in the downstream of HRB was remarkably higher than that of the upstream at all drought scenarios. Additionally, SY showed the highest drought propagation threshold at moderate and severe drought scenarios, while XJWP at extreme drought scenario.

1 Introduction

Drought is a complex natural disaster caused by the abnormal decrease of precipitation, which has a grievous fatal effects on agriculture, ecology and social economy (Oladipo, 1985; Huang and Chou, 2008; Huang et al., 2015; Fang et al., 2019; Guo

1 et al., 2019). Compared with other natural disasters, droughts cause much more severe damages than other natural disasters
2 because of their extensive spatial impact and generally longer duration (Mishra and Singh, 2010). In the last few decades,
3 remarkable changes in global climate and environment aggravated the occurrence of hydrological extreme events
4 characterized by drought (Wilhite and Glantz, 1985; Palmer and Räisänen, 2002; Kunkel, 2003; Beniston and Stephenson,
5 2004; Christensen and Christensen, 2004; Leng et al., 2015).

6 Hydrological drought, mainly lagged the occurrence of meteorological drought, manifests in the case of long-term lack of
7 precipitation, resulting in the overall water supply shortage in terms of river flow, groundwater and reservoir storage
8 (Vicente-Serrano and LópezMoreno, 2005; Van Lanen et al., 2013; Joetzjer et al., 2013). Developing reliable drought indices
9 can reveal the hydrological drought status of the basin well (Mishra and Singh, 2011; Wang et al., 2020). Standardized
10 runoff Index (SRI), established based on runoff variation, is commonly applied in hydrological drought evaluation and has
11 been widely used in drought frequency analysis and drought risk management (Vicente-Serrano et al., 2012; Rivera et al.,
12 2017; Chen et al., 2018; Xu et al., 2019; Yang et al., 2020). Therefore, based on the SRI, the spatio-temporal evolution of
13 drought events can be quantitatively revealed. Run theory (Yevjevich, 1967), a time series analysis method, is widely
14 applied to identify drought events and extract drought characteristic values, such as drought duration and severity (Kim et al.,
15 2011; Liu et al., 2016a, 2016b; Wu et al., 2017; Sun et al., 2019). The copula function can combine multiple drought
16 characteristic variables well, which provides an effective method for multivariate frequency analysis (Lee et al., 2013; Vyver
17 and Bergh 2018; Dash et al., 2019; Lindenschmidt and Rokaya, 2019). Thus, the copula function with the highest goodness
18 of fit would be selected to establish the joint distribution of drought duration and drought severity, and calculate the return
19 period of hydrological drought, which has significant practical significance for regional hydrological drought prediction
20 (Kao and Govindaraju, 2009; Mirabbasi et al., 2012).

21 In general, hydrological drought is a response to the accumulation of meteorological drought conditions. Many scholars
22 have made lots of attempts to study the relationship between hydrological drought and meteorological drought (Pandey and
23 Ramasastri, 2001; Van Loon et al., 2012; Leng et al., 2015; Barker et al., 2016; Sattar et al. 2019). Amongst these previous
24 studies, more efforts have been focused on the calculation of drought propagation time (Lorenzo-Lacruz et al., 2013; Huang
25 et al., 2017; Gevaert et al., 2018). There are few studies on the intensity of the meteorological drought that triggers
26 hydrological drought with different levels. Guo et al. (2020b) explored the drought propagation thresholds of meteorological
27 drought for triggering hydrological drought at various levels based on the copula-based conditional probability model. The
28 duration and severity of meteorological drought were used as the detection values to trigger hydrological drought. However,
29 it is not ideal to use drought duration or severity as meteorological drought detection value for triggering hydrological
30 drought because of its relative absolute and inconvenient monitoring. Guo et al. (2020a) proposed a drought propagation
31 threshold model based on Bayesian networks, which took cumulative precipitation deficit as the condition and single time

1 scale SRI as the target to clarify the impact of large reservoirs on watershed drought tolerance by calculating cumulative
2 deficit rainfall triggering different levels of hydrological drought. However, although single time scale SRI can capture
3 hydrological regime changes sensitively and accurately, a severe drought event usually lasts for several months. Therefore, it
4 is not accurate to take the cumulative precipitation deficit calculated with a single time scale SRI as the threshold for
5 triggering hydrological drought in the drought propagation threshold model. And, it is highly necessary to select appropriate
6 hydrological and meteorological drought factors as targets and conditions to improve the drought propagation threshold
7 model so as to obtain more accurate propagation threshold for triggering different scenarios of hydrological drought.

8 Thus, in this study, SRI and Standardized Precipitation Index (SPI) were implied to characterize meteorological drought
9 and hydrological drought, respectively (McKee et al., 1993; Shukla and Wood, 2008). The run theory was applied to SRI
10 series to identify hydrological drought events and capture their corresponding drought characteristic values, drought duration
11 and intensity. SRI and drought characteristic values were implied to quantitatively reveal the evolution characteristics of
12 hydrological drought. Meanwhile, the copula functions with the highest goodness of fit were selected to establish the joint
13 distribution of drought duration and drought severity, and calculate the return period of hydrological drought. Then, the
14 Pearson correlation coefficients between 1-month SRI and multi-time scale SPI were calculated to determine the drought
15 propagation time from meteorological drought to hydrological drought (i.e. PTMH) (Barker et al., 2016; Huang et al., 2017;
16 Fang et al., 2020). Based on the PTMH and drought duration, the cumulative precipitation deficit of each hydrological
17 drought event was determined, which was applied to characterize meteorological drought. The drought duration and severity
18 were used to describe a single hydrological drought event. Furthermore, based on the copula function and Bayesian model, a
19 improved drought propagation threshold model was established, including the cumulative precipitation deficit, drought
20 duration and drought intensity. Finally, the drought propagation threshold interval would be determined according to the
21 magnitude of the conditional probability of occurrence of hydrological drought events under different cumulative
22 precipitation deficit conditions.

23 In general, the primary objectives of this paper are: (1) to reveal the spatiotemporal evolution characteristics of
24 hydrological drought; (2) to select the best-fit copula and calculate the hydrological drought return period; (3) to determine
25 the PTMH; (4) to establish drought propagation threshold model based on Bayesian network to determine the propagation
26 thresholds for triggering different scenarios of hydrological drought.

27 **2 Study region and data**

28 The HRB, as presented in Fig. 1, is located in Liaoning Province, NE China and covers an area of 11,481 km², among which
29 the hilly area occupies 67% and plain area 33%. The basin belongs to the temperate semi-humid and semi-arid monsoon
30 climate, with four distinct seasons and the same season of rain and heat, and weak climate differences within the basin. The

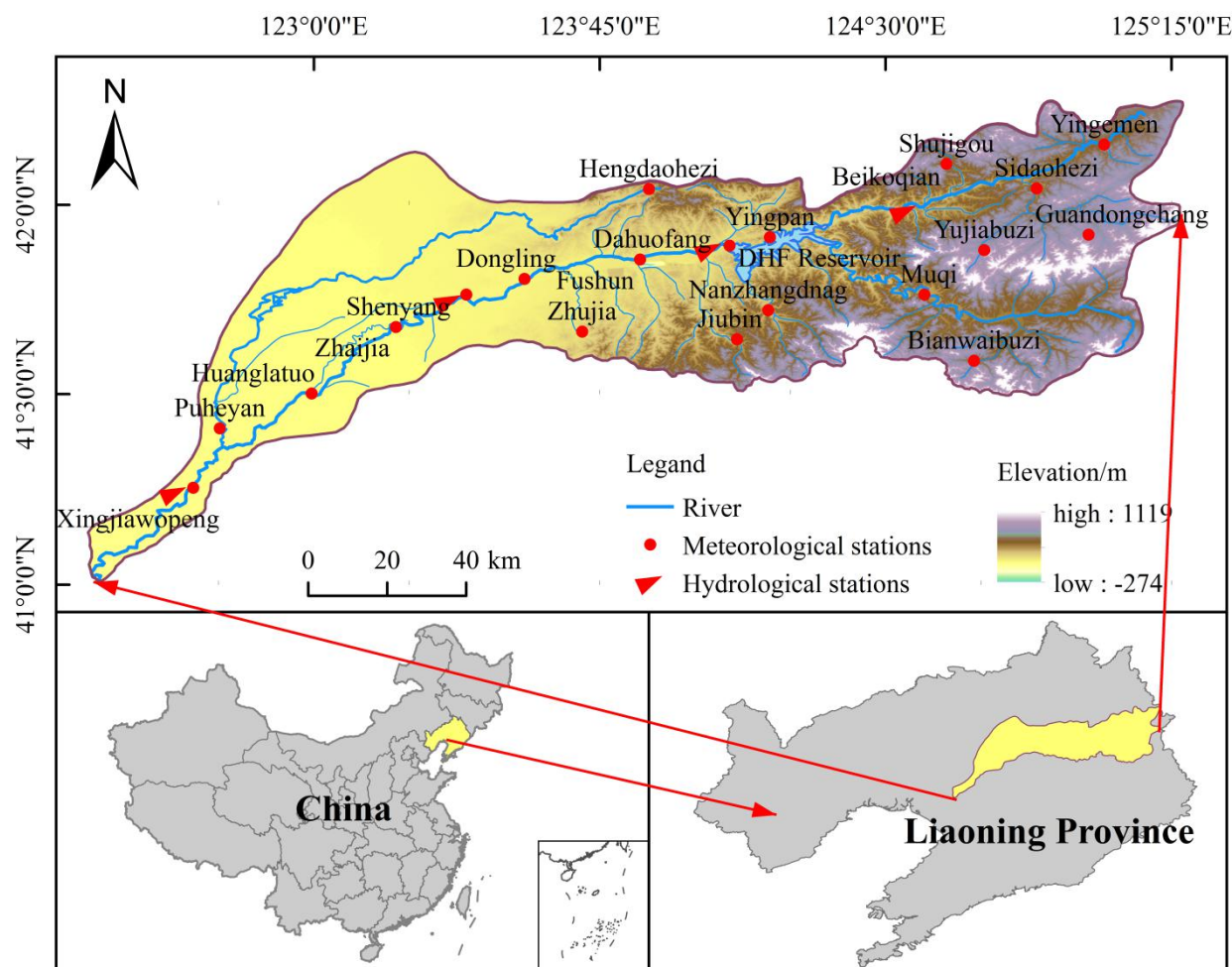
1 warm and wet air flow from the low latitude tropical monsoon circulation prevails in the summer brings more rainy days,
2 while the Siberia-Mongolia high pressure dry cold continental air flow occurs during the winter, prevailing north wind and
3 northwest wind, resulting in low temperature and less precipitation. The multi-year average precipitation is approximately
4 780 mm, with obvious seasonal characteristics, and the precipitation in the main flood season (July to August) accounts for
5 about 48.5% of the annual precipitation.

6 Dahuofang (DHF) reservoir, located in the middle and upper reaches of HRB, is a large-scale water control project, with a
7 total storage capacity of 2.268 billion cubic meters. DHF reservoir plays a vital function in flood control and water supply, as
8 well as for power generation and fish farming. Since the operation of DHF Reservoir in 1958, the irrigation, the river
9 ecosystem of the region and the hydrological condition of the river channel have been greatly affected. Three hydrological
10 stations in HRB were selected from upstream to downstream: Dahuofang (DHF), Shenyang (SY), and Xingjiawopeng
11 (XJWP) stations to explore the spatial distribution of hydrological drought in this study. The three hydrological stations
12 selected are located downstream of each basin, so the hydrological information of each basin can be reflected by the status of
13 the corresponding hydrological stations (Fu et al., 2004). They represent the hydrological conditions of above DHF, DHF to
14 SY and SY to XJWP, respectively. The monthly runoff dates of these four hydrological stations and monthly precipitation
15 data of the twenty meteorological stations during 1967-2019 were adopted in this study, which were collected from the
16 Hydrological Data of Liao River Basin from the Year Book of Hydrology P.R.CHINA. Additionally, Thiessen polygon
17 method was applied to calculate the precipitation of meteorological stations to get the corresponding area precipitation of
18 each hydrological station.

19 **3 Methodology**

20 **3.1 Standardized precipitation index (SPI) and Standardized runoff Index (SRI)**

21 In this paper, meteorological and hydrological drought were characterized by SPI and SRI, respectively. SPI was proposed
22 by McKee et al. (1993) to characterize the drought conditions in Colorado, USA, and it has been recommended by the World
23 Meteorological Organization as the primary meteorological drought index to be used. SRI was proposed by Shukla and
24 Wood (2008) to reflect drought from the perspective of hydrology. Both SPI and SRI, established based on historical
25 precipitation and runoff data respectively, can monitor droughts over a range of time scales. SPI and SRI were calculated in
26 similar calculation procedures, in which gamma distribution were used to describe the variation of precipitation and runoff,
27 respectively. The cumulative probability of precipitation / runoff can be obtained based on gamma distribution, and then
28 cumulative probability was converted to the standard normal distribution to obtain SPI / SRI values. More details calculation
29 can be found in Huang et al. (2017). According to the SPI/SRI values, droughts are classified into five grades. The criteria
30 are shown in Table 1.



1
2 **Figure. 1** Locations of the HRB, DHF reservoir, and the meteorological and hydrological stations.

3 **Table. 1** Definition of drought conditions based on the SPI (SRI).

State	Condition	Criterion
1	Non-drought	$SPI(SRI) > -0.5$
2	Mild drought	$-1.0 < SPI(SRI) \leq -0.5$
3	Moderate drought	$-1.5 < SPI(SRI) \leq -1.0$
4	Severe drought	$-2.0 < SPI(SRI) \leq -1.5$
5	Extreme drought	$SPI(SRI) \leq -2.0$

4 **3.2 The Mann-Kendall trend test method**

5 The Mann-Kendall (M-K) trend test (Mann, 1945; Kendall, 1975), a non-parametric statistical testing method, is widely used
6 to accessing the trends of hydrological variables. Therefore, this paper adopted M-K method to investigate the trend
7 characteristics of hydrological drought on the seasonal, and annual scales in the HRB during 1967-2019 with the significance
8 level of 0.05 and the corresponding $|U| = 1.96$. The calculation procedure of the M-K method was described in Huang et al.
9 (2016).

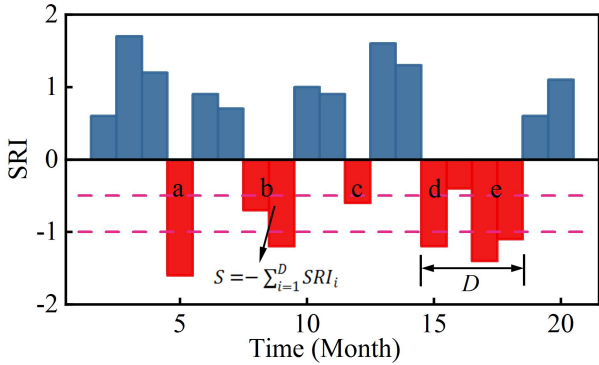
10 **3.3 Run theory and copula functions**

1 Run theory is a time series analysis method which is widely applied to identify drought events and extract drought
 2 characteristic values (Zhao et al., 2017; Sun et al., 2019). In this paper, based on the three thresholds SRI_0 (-0.5), SRI_1 (-1.0)
 3 and SRI_2 (0.0), the run theory was used to identify three drought factors, namely drought event, duration and severity, from
 4 the 1-month scale SRI sequence. Fig. 2 shows the process of drought recognition based on the threshold method, and the
 5 specific identification process is as follows:

6 (1) Drought characteristics are considered to appear when SRI value is less than SRI_0 . Hence, it is preliminarily believe
 7 that drought occurs during the period from t_1 when SRI value is equal to or less than SRI_0 to t_2 when SRI value is equal to
 8 SRI_0 or even larger. The run duration (i.e. t_2-t_1) and the absolute value of the accumulated SRI during the drought duration
 9 are identified as drought duration (D) and drought severity (S), respectively. For example, five drought processes (i.e. a, b, c,
 10 d and e) can be recognized in Fig. 2.

11 (2) On the basis of (1), if a drought has a duration of just one month, it is considered as a drought event only when its
 12 corresponding SRI value is less than SRI_1 , otherwise, it is not (c).

13 (3) If a drought event (e) occurs one month later than the preceding one (d), and the SRI value in between is less than SRI_2 ,
 14 these two drought events (d and e) are regarded as one combined drought event, otherwise, they are considered as two
 15 independent drought events. The severity and duration of the combined drought event is $S=S_d+S_e$, and $D=D_d+D_e+1$,
 16 respectively.



17 **Figure. 2** Drought identification process and definition of drought characteristic variables.

18 The sequences of drought duration and severity determined by the run theory were then fitted by five common functions,
 19 including Gamma (GAM), Generalized extreme value (GEV), Exponential (EXP), Lognormal (Logn) and Weibull (WBL)
 20 distributions (Rad et al., 2017; Wang et al., 2020). And, Kolmogorov-Smirnov (K-S), Root mean square error (RMSE) and
 21 AIC test were employed to identify the best-fit marginal distribution functions. Copula function is a multidimensional joint
 22 distribution function defined in $[0,1]$, and can integrate marginal distributions of several dependent random variables to
 23 structure a joint probability distribution with multiple features. Previous studies have proved that the copula function is a
 24 high-efficiency tool for multivariate probability analysis of drought (Hao and Singh, 2015; Salvadori and De Michele, 2015;
 25 Ren et al., 2020). Its equation is expressed as follows:
 26

$$C(u, v) = \varphi^{-1}(\varphi(u), \varphi(v)) \quad (1)$$

where $C(u, v)$ represents the copula function combining two random variables u and v ; and φ is convex function.

In this study, the dependency structures of drought duration and severity were modeled with the commonly used binary copula functions, including Gumbel–Hougaard, Clayton, Frank, t and Normal copula (Lee et al., 2013 and Wang et al., 2020). Kolmogorov-Smirnov (K-S), Cramér-von Mises (C-M) (Genest et al., 2011 and Rad et al., 2017), RMSE and AIC test were applied to select the best copula function with highest goodness of fit (GOF). In addition, several joint probability expressions corresponding to bivariate return periods were used to further explore the occurrence frequency of hydrological drought. The expressions of joint probability are defined as:

$$T_{and} = \frac{E(L)}{P[(D>d \cap (S>s))]} = \frac{E(L)}{1-F_D(d)-F_S(s)+F(d,s)} \quad (2)$$

$$T_{or} = \frac{E(L)}{P[(D>d) \cup (S>s)]} = \frac{E(L)}{1-F(d,s)} \quad (3)$$

where $E(L)$ denotes the expected value of drought interval and $F_D(d)$ and $F_S(s)$ are marginal cumulative density function of drought duration and severity, respectively. $F(d,s)$ is joint distribution function of drought duration and severity. T_{and} is the return period of drought events that both exceed the thresholds of duration ($D \geq d$) and severity ($S \geq s$) and T_{or} is return period of drought events that considered exceed the threshold of duration ($D \geq d$) or severity ($S \geq s$).

3.4 The drought propagation time

In general, hydrological drought is a response to the accumulation of meteorological drought conditions. Generally, the change of hydrological regime can be characterized sensitively by the single time scale SRI, and the accumulation of meteorological drought in the preceding n months can be reflected by the n time scale SPI. The time scale of SPI with the highest correlation with the single time scale SRI is regarded as drought propagation time (i.e. PTMH) (Barker et al., 2016; Huang et al., 2017; Fang et al., 2020). Therefore, Pearson correlation between monthly scale SRI and multi-time scale SPI (1-24 months) was adopted in this study to determine the PTMH, which is symbolize as T_P .

3.5 The calculation of drought propagation threshold

Bayesian network, a probabilistic graph model, is widely used in drought impact assessment (Sattar et al., 2019; Guo et al., 2020a). Therefore, a threshold model of drought propagation based on Bayesian network is established in this study.

Suppose $X(x_1, x_2, \dots, x_n)$ and $Y(y_1, y_2, \dots, y_n)$ are two random variables, with X and Y as conditions and targets respectively.

Then, in the case of $X \geq u$, the probability of $Y \geq v$ can be expressed as:

$$P(Y \geq v | X \geq u) = \frac{P(X \geq u, Y \geq v)}{P(X \geq u)} = \frac{1-x(u)-y(v)+C(x(u), y(v))}{1-x(u)} \quad (4)$$

1 where $C(x(u), y(v))$ represents the joint cumulative probability of $X \leq u$ and $Y \leq v$; $x(u)$ and $y(v)$ denote the cumulative
 2 probability of $X \leq u$ and $Y \leq v$; x and y are the marginal cumulative distribution of two random variable X and Y . In addition,
 3 when $u_2 \geq X \geq u_1$, the probability of $Y \geq v$ is expressed as:

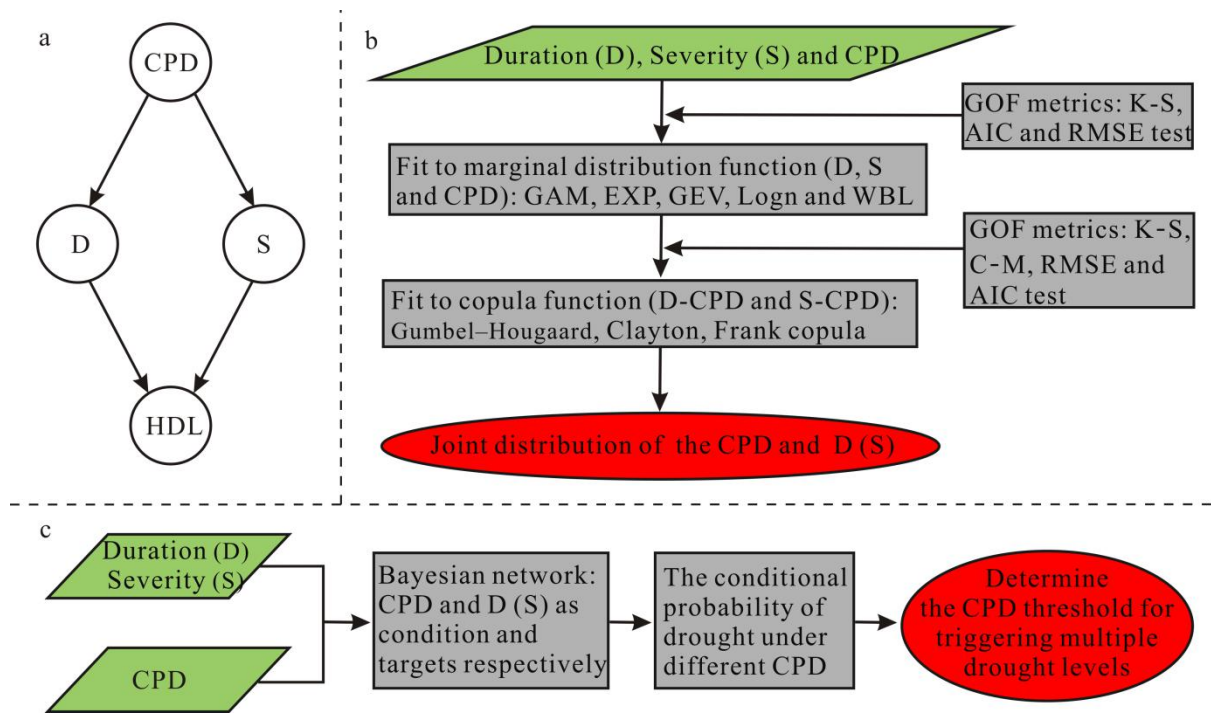
$$\begin{aligned}
 4 \quad P(Y \geq v | u_1 \leq X \leq u_2) &= \frac{P(Y \geq v, u_1 \leq X \leq u_2)}{u_1 \leq X \leq u_2} = \frac{x(u_2) - x(u_1) - C(x(u_2), y(v)) + C(x(u_1), y(v))}{x(u_2) - x(u_1)} \\
 5 \quad &= 1 - \frac{C(x(u_2), y(v)) - C(x(u_1), y(v))}{x(u_2) - x(u_1)} \quad (5)
 \end{aligned}$$

6 where u_1 and u_2 are the upper and lower limits of the given interval.

7 Fig 3a shows the graphical model of Bayesian network. It describes the causal relationships among the cumulative
 8 precipitation deficit (CPD, mm), drought duration (D), severity (S) and hydrological drought levels (HDL). The response
 9 variable Y here is hydrological drought with two components duration (D) and severity (S), and the feature variable X that
 10 characterizes Y is cumulative precipitation deficit (CPD). Among them, the CPD is the cumulative precipitation deficit of
 11 each hydrological drought event during the PTMH, which is defined as (Guo et al., 2020a):

$$12 \quad CPD_n = - \left(\max_{D \geq t \geq 1} \sum_{i=t-T_p+1}^t (P_i - \bar{P}_m) + \sum_{i=1}^{D-t} (P_i - \bar{P}_m) \right) \quad (6)$$

13 where CPD_n is the corresponding CPD for the n th drought; P_i denotes the precipitation during the period of i ; \bar{P}_m represents
 14 the average precipitation of the m th month. As for Fig 3b showed, according to the method of determining the marginal
 15 distribution described in Section 3.3, the best-fit marginal distribution function of CPD was identified. The commonly used
 16 bivariate theoretical copula functions, including Clayton, Frank, and Gumbel copula were considered for modeling the
 17 dependence structure between CPD and drought duration and severity, respectively. And, K-S, C-M, RMSE and AIC test
 18 were applied to select the GOF copula function. Then, the joint distributions of CPD and D (S) were established based on the
 19 GOF copula functions. As shown in Fig 3c, in this model, the drought duration and severity of each drought event are taken
 20 as the target, respectively, and the corresponding CPD is identified as the condition. The conditional probability of
 21 hydrological drought under different CPD conditions would be calculated. Then, the CPD corresponding to the confidence
 22 level of 0.95 was identified to determine the drought propagation threshold for triggering hydrological drought events.

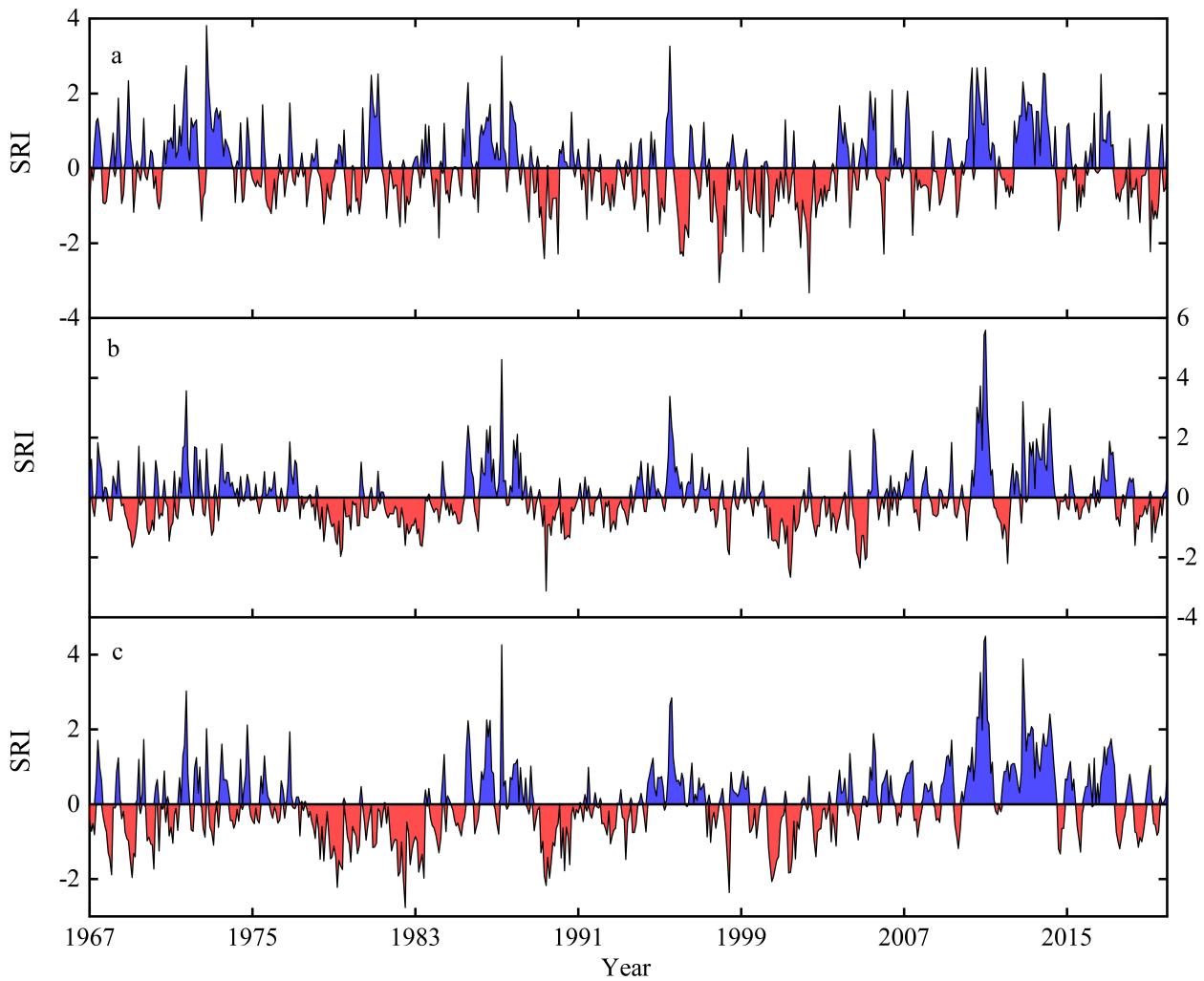


1
2 **Figure. 3** The schematic of determining the drought propagation threshold based on bivariate copula and Bayesian network.
3 (a) The graphical model of Bayesian network about CPD, D, S and HDL; (b) Modelling the dependence of CPD on
4 hydrological drought; (c) Quantifying the CPD threshold under multiple drought levels.

5 4 Results and discussions

6 4.1 Spatiotemporal evolution of hydrological drought

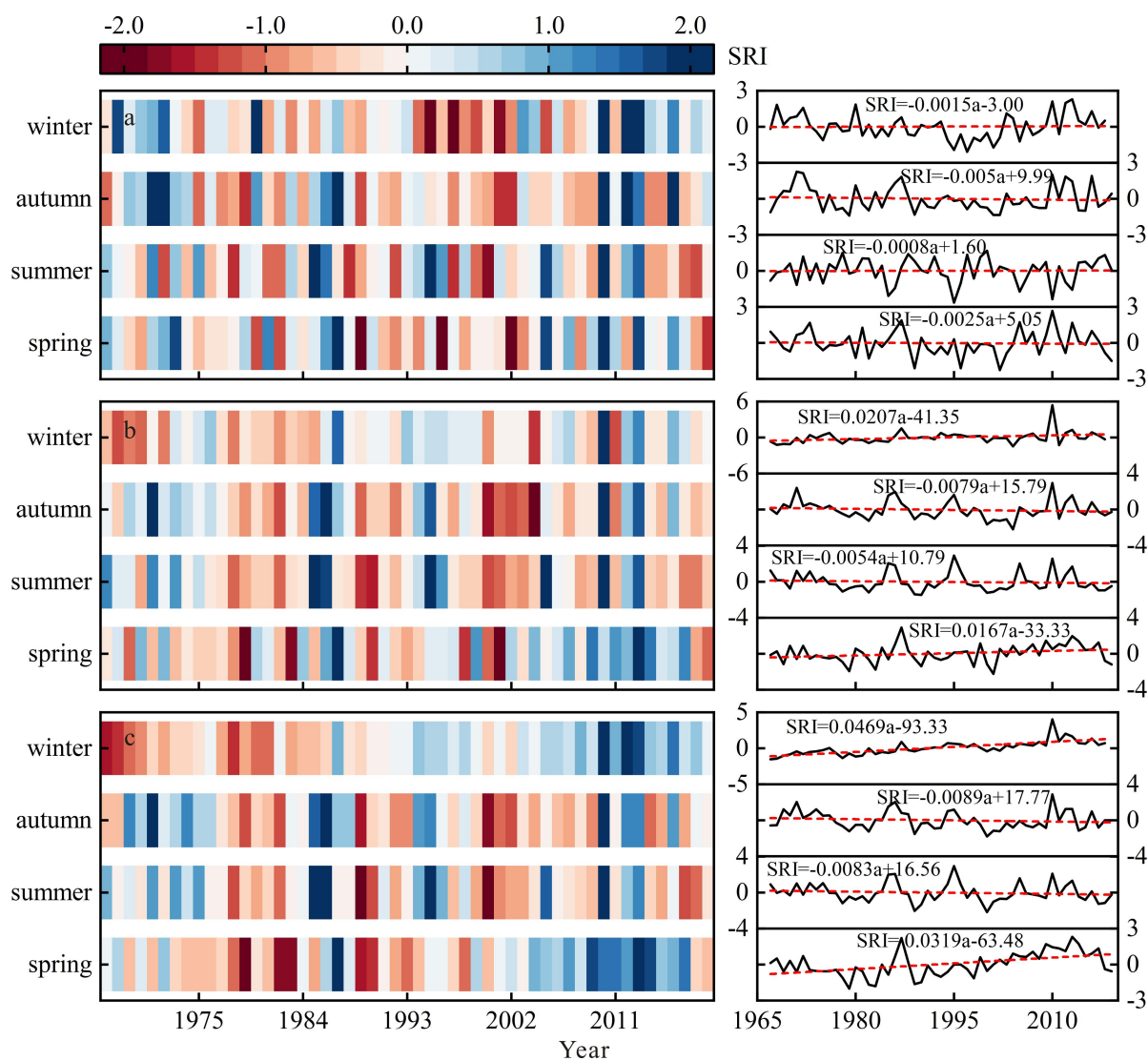
7 For hydrological drought, the change of hydrological regime can be sensitive and accurately captured by single time scale
8 SRI. Therefore, the single time scale SRI is applied to study the spatiotemporal evolution of hydrological drought. Fig. 4
9 depicts the temporal variation trend of hydrological drought based on the monthly scale SRI in HRB from 1967 to 2019,
10 which presented difference temporal evolution characteristics in each sub-basin. It is clear from Fig. 4a that the SRI
11 sequence showed a non-significant decreasing trend in the DHF, which indicated that the drought showed slight
12 strengthening trend in DHF. The significant strengthening trend of drought occurred from March 1991 to September 2004,
13 with average SRI value of -0.54 and minimum of -3.33. Fig. 4 (b, c) presents that the temporal evolution characteristics of
14 hydrological drought were similar in SY and XJWP, showed alternate characteristics of drought and flood. Droughts
15 occurred mainly from May 1977 to April 1984, November 1988 to November 1993 and May 2000 to September 2003 in SY,
16 with average SRI value of -0.84, -0.56 and -0.70, respectively. Similarly, droughts occurred mainly from April 1978 to May
17 1985, November 1988 to July 1993 and March 2000 to March 2005 in XJWP, with average SRI value of -0.57, -0.50 and
18 -0.81, respectively.



1
 2 **Figure. 4** Temporal variation of hydrological drought based on monthly scales in HRB during 1967-2019. (a) - (c) denote DHF, SY and
 3 XJWP, respectively.

4 The multi-timescale SRI applies to describe the mean hydrological regime during the preceding few months. Therefore,
 5 the SRI-3 and SRI-12 were calculated to analyze the seasonal and annual variation trend of hydrological drought. The SRI-3
 6 values in February, May, August and November were applied to describe the variations of hydrological drought in winter,
 7 spring, summer and autumn, respectively. Fig. 5 presents the temporal variation of hydrological drought at seasonal scales in
 8 HRB from 1967 to 2019. From the interannual perspective, the drought trend was different in sub-regions, with the linear
 9 slope of SRI changed from $-0.089/10a$ to $0.469/10a$. SRI showed a decreasing trend at spring, summer and autumn in DHF,
 10 with the linear slope of SRI were $-0.025/10a$, $-0.008/10a$ and $-0.050/10a$, which indicated that drought was aggravating at
 11 spring, summer and autumn. The linear slope of SRI was $0.167/10a$ and $0.207/10a$ at spring and winter, while $-0.054/10a$ and
 12 $-0.079/10a$ at summer and autumn in SY, indicating that drought was strengthening in summer and autumn and decreasing in
 13 spring and winter. Similar to the temporal characteristics of SY, drought showed a strengthening trend in summer and
 14 autumn, while a decreasing trend in spring and winter in XJWP with the linear slope of SRI were $-0.083/10a$, $-0.089/10a$,
 15 $0.319/10a$ and $0.469/10a$, respectively. Moreover, it can be observed from Fig. 5 that both continuous drought and
 16 drought-flood abrupt alternation may occur in HRB within the year.

1 In order to further explore the temporal evolution characteristics of hydrological drought, the trend characteristic U values
 2 of M-K trend test of SRI-3 and SRI-12 was calculated. Table 2 shows the calculation results of trend characteristic value U at
 3 seasonal and annual scales. It is clear from Table 2 that the characteristics of drought trends in different periods and stations
 4 are obviously different. On the annual scale, the U value of DHF, SY and XJWP stations were -0.84, -0.37 and -0.09,
 5 indicating a non-significant strengthening trend of drought in the HRB. On the seasonal scale, the U values of each
 6 sub-basin in summer and autumn were less than zero, which indicated that drought was strengthening in summer and autumn
 7 in HRB. The U values of DHF were less than zero in spring and winter, which indicated that drought showed a strengthening
 8 trend in spring and winter at DHF. However, the U values of SY and XJWP stations were 2.15, 2.34, 3.67 and 6.64 in spring
 9 and winter, respectively. These trend characteristic U values passed the significance test of $\alpha = 0.05$, indicated that the
 10 drought showed a significant decreasing trend in spring and winter at the SY and XJWP of HRB. All in all, the drought at
 11 DHF showed an strengthening in all seasons and showed an strengthening trend in summer and autumn, while an decreasing
 12 trend in spring and winter at SY and XJWP, which can be confirmed with the conclusions of previous section.



13

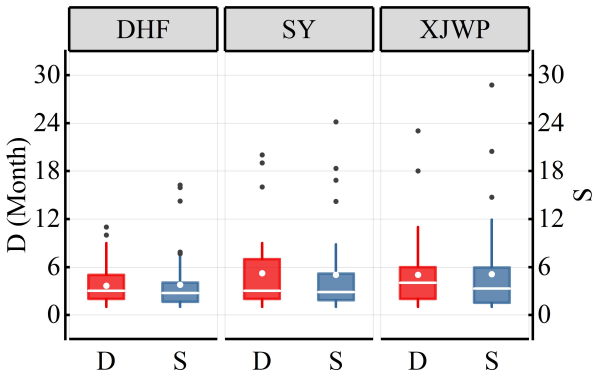
1 **Figure. 5** Temporal variation of hydrological drought at seasonal scales in the HRB from 1967 to 2019. (a)-(c) denotes DHF, SY and
 2 XJWP, respectively.

3 **Table. 2** U values of SRI at the seasonal and annual scales in the HRB during 1967-2019.

Sub-region	DHF		SY		XJWP	
	U value	Trend	U value	Trend	U value	Trend
Spring	-0.52	downward	2.15	upward	3.67	upward
Summer	-0.4	downward	-1.47	downward	-1.49	downward
Autumn	-0.95	downward	-1.46	downward	-1.15	downward
Winter	-0.11	downward	2.34	upward	6.64	upward
Year	-0.84	downward	-0.37	downward	-0.09	downward

4 The bold letters denote that the U values passed the MK trend test of $\alpha = 0.05$.

5 Based on the run theory, three drought factors, namely drought events, duration and severity, were identified from the
 6 1-month scale SRI sequence. Drought events which were detected sum up to 133 in 3 districts of HRB during 1967-2019.
 7 DHF was most frequently affected by drought, with a total of 57 drought events, followed by XJWP and SY with 39 and 37
 8 drought events, respectively. The box chart of drought duration and severity was drawn, and the spatial distribution of
 9 drought was discussed (Fig. 6). Fig. 6 shows that districts with the mean of drought duration more than 5 months included
 10 SY and XJWP, while the median drought duration of XJWP was greater than DHF and SY. Besides, SY and XJWP have
 11 experienced extremely long duration drought events lasting more than 23 months. The districts in the west (XJWP) and
 12 center (SY) were more likely experience longer drought events and the longer-duration drought events was most likely to
 13 occur in central regions. Drought severity and drought duration maintained a highly consistency. The highest drought
 14 severity occurred in XJWP and the mean drought severity of DHF was less than XJWP and SY (Fig. 6). In summary,
 15 western and center of the HRB were vulnerable district to hydrological drought, where the drought duration and severity
 16 were more serious than in eastern (DHF) districts. Nevertheless, the eastern region of the HRB was more sensitive to
 17 short-duration drought, which were dominated by two-month and three-month drought events.



18 **Figure. 6** Box chart of duration and severity of hydrological drought.

20 **4.2 Periodicity analysis**

1 In order to grasp the occurrence frequency of hydrological drought in HRB , the periodicity was analyzed by calculating the
 2 return period. In this study, five common functions including Gamma, EXP, GEV, Logn, and WBL, were used to fit the
 3 sequence of duration and severity of hydrological drought events in the three sub-basins of HRB. AIC, RMSE and K-S test
 4 were applied to select the best-fit marginal distribution, and the results were shown in Table 3. Table 3 illustrates that the
 5 optimal distribution for different drought characteristics passed the K-S test ($\alpha = 0.05$) in all the four sub-regions. The joint
 6 distribution of drought duration and severity in the HRB was determined with the application of copula functions. According
 7 to the values of K-S, C-M, RMSE and AIC, the GOF copula functions were selected as the best joint distribution of drought
 8 duration and severity in the HRB (Table 4).

9 **Table. 3** Optimum marginal distribution function of drought characteristics (D, S and CPD).

Sub-region	Drought characteristics	Optimal distribution	AIC	RMSE	K-S
BKQ	Duration (D)	EXP	-283.37	0.068	0.190*
	Severity (S)	Logn	-310.04	0.053	0.123*
	CPD	GAM	-374.31	0.029	0.062*
DHF	Duration (D)	EXP	-333.89	0.053	0.094*
	Severity (S)	GEV	-386.58	0.033	0.072*
	CPD	WBL	-404.9	0.028	0.061*
SY	Duration (D)	EXP	-204.75	0.061	0.148*
	Severity (S)	GEV	-249.64	0.033	0.098*
	CPD	GEV	-239.9	0.038	0.098*
XJWP	Duration (D)	GEV	-239.43	0.045	0.105*
	Severity (S)	Logn	-251.49	0.039	0.106*
	CPD	GEV	-236.55	0.047	0.113*

10 “*” denote that the optimal distribution passed the K-S test of $\alpha = 0.05$.

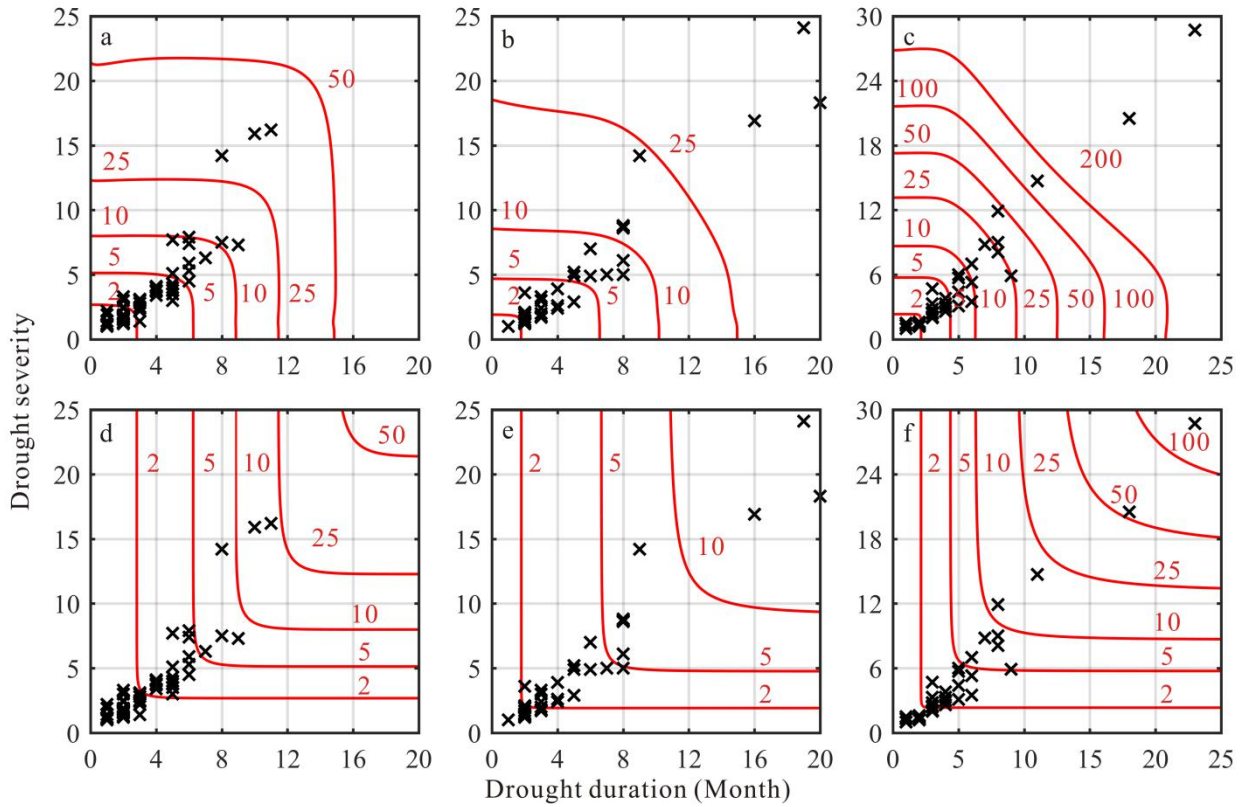
11 **Table. 4** GOF evaluation of different copula functions about drought duration and severity in the HRB.

Copulas	GOF test	DHF	SY	XJWP
Clayton	K-S	0.119	0.129	0.115
	C-M	0.140	0.079	0.084
	RMSE	0.049	0.046	0.046
	AIC	-340.68	-225.69	-237.35
Gumbel–Hougaard	K-S	0.092	0.099	0.141
	C-M	0.079	0.058	0.098
	RMSE	0.037	0.040	0.050
	AIC	-373.13	-237.05	-231.59
Frank	K-S	0.103	0.109	0.138
	C-M	0.094	0.051	0.089
	RMSE	0.041	0.037	0.048
	AIC	-363.30	-241.88	-235.26
Normal	K-S	0.091	0.107	0.131
	C-M	0.082	0.056	0.088
	RMSE	0.038	0.039	0.048
	AIC	-371.35	-238.47	-235.51

	K-S	0.091	0.106	0.126
	C-M	0.080	0.059	0.088
t	RMSE	0.038	0.040	0.048
	AIC	-372.16	-236.11	-235.60

1 Bold letters represent the optimal copula functions.

2 Fig. 7 shows the contour plots of return period levels of drought events based on the optimal copula, and the return period
3 T_{and} and T_{or} of drought events in each sub-region can be observed. The drought return period increased with the increase of
4 drought duration and severity in the HRB. For the same drought event, return period T_{and} would be higher than T_{or} .
5 Meanwhile, regarding the same return period, drought duration and severity from large to small were SY, DHF and XJWP,
6 respectively. In DHF, the drought occurred from September 2001 to July 2002 was the most severe, lasting 11 months, with
7 severity of 16.2, and return period T_{and} and T_{or} were 33 years and 17 years, respectively. In SY, the most severe drought
8 happened from May 2000 to November 2001, lasting 19 months, with severity of 24.1, and return period T_{and} and T_{or} were
9 152 years and 24 years, respectively. Similarly, the drought occurred from August 1981 to June 1983 was the most severe in
10 XJWP, lasting 23 months, with severity of 28.7, and return period T_{and} and T_{or} were 371 years and 89 years, respectively.



11

12 **Figure. 7** The return periods T_{and} and T_{or} of 1-month scale drought events in DHF (a and d), SY (b and e) and XJWP (c and f).

13 Besides, according to the univariate empirical frequency of drought duration and severity, three typical drought scenarios
14 were selected to analyze the return periods. The scenarios corresponding to the empirical frequency of 0.50, 0.25 and 0.05 of
15 the univariate were defined as moderate, severe and extreme drought (i.e. Moderate drought is defined as the drought when
16 the duration and intensity of drought is greater than the median corresponding to 0.5). Table 5 exhibits the drought return

1 periods T_{and} and T_{or} under different drought scenarios and their corresponding drought duration and drought severity in DHF,
 2 SY and XJWP. For moderate drought, the return period T_{and} and T_{or} had the same regularity in DHF, SY and XJWP, with the
 3 largest value in SY, followed by XJWP and DHF. As for severe drought, the distribution of T_{and} and T_{or} about severe and
 4 extreme drought were consistent in DHF, SY and XJWP, which showed that SY has the highest return period T_{or} , followed
 5 by XJWP and DHF, while the return period T_{and} in XJWP was greater than SY and DHF. It should be noted that the drought
 6 presented the characteristics of smaller return period with high drought duration and large severity in eastern of the HRB. It
 7 is foreseeable that eastern districts will be more likely to suffer from more serious drought events.

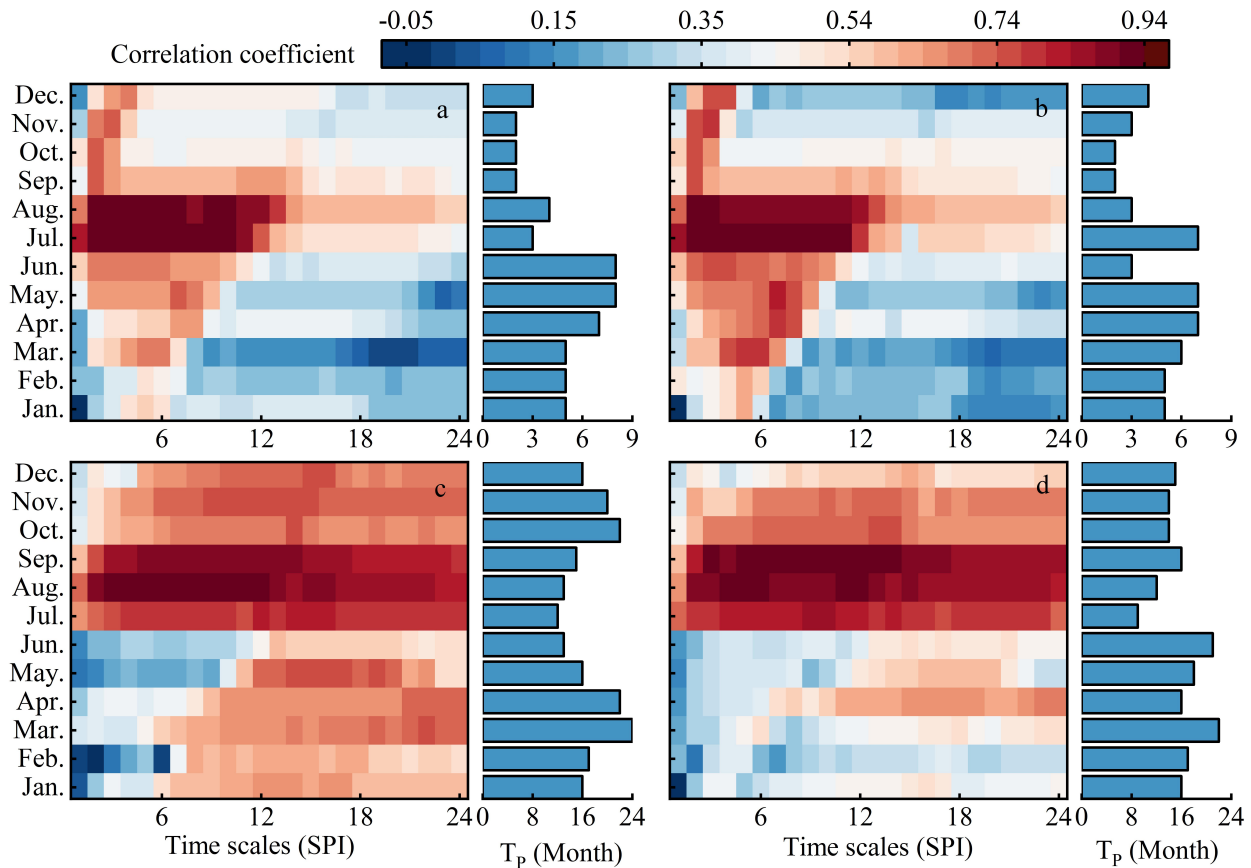
8 **Table. 5** The drought return periods T_{and} and T_{or} under different drought scenarios and their corresponding drought factors in HRB.

Sub-region	Drought scenario	T_{and} (Year)	T_{or} (Year)	Drought duration (Month)	Drought severity
DHF	Moderate drought	2.3	1.7	3	2.6
	Severe drought	4.5	3.1	5	4.3
	Extreme drought	22.8	14.9	11	11.9
SY	Moderate drought	3.3	2.7	4	2.8
	Severe drought	6.7	4.8	7	5.3
	Extreme drought	71	18.6	16	20.7
XJWP	Moderate drought	3.2	2.6	4	3.5
	Severe drought	7.3	4.4	6	6.1
	Extreme drought	79	16.3	13	13.8

9 4.3 The propagation from meteorological to hydrological drought

10 Based on the superiority of SPI that it can be calculated at multi-time scales, the T_p were determined by calculating the
 11 Pearson correlation coefficient between the monthly SRI and the multi-time SPI. The T_p was indicated by the month with the
 12 strongest correlation. However, the correlation is high for a large variety of SPI time scales in some months, which makes
 13 the identification of T_p values highly uncertain. Therefore, in order to overcome this issue, the uncertainty of the correlation
 14 coefficients was calculated. And the T_p was expressed on SPI time scale with strong correlation and low uncertainty. The
 15 Pearson correlation coefficient and the T_p of DHF, SY and XJWP were shown in Fig. 8. It can be seen from Fig. 8 that the T_p
 16 of SY and XJWP was significantly higher than that of DHF in all months. In order to further confirm the difference in T_p
 17 between the upstream and downstream of DHF reservoir, and to analyze the causes of the difference, the T_p at Beikouqian
 18 (BKQ) was also analyzed. The locations of the four hydrological stations are shown in Fig. 1. The BKQ is located upstream
 19 of the DHF reservoir, while SY and XJWP are successively arranged in the downstream of DHF reservoir. As shown in Fig.
 20 1, the BKQ and DHF are located in the eastern part of the HRB with mountainous terrain, while SY and XJWP are in the
 21 western plain. The slope of BKQ and DHF is greater than that of other sub-basins, indicating that the underlying surface has
 22 less water retention and buffer capacity than other regions. Meanwhile, the runoff process in the downstream of the reservoir
 23 can be redistributed on the spatial and temporal scale through the operation of the reservoir (Shiklomanov et al., 2000;

1 Chang et al., 2019). Therefore, under the combined action of stronger water retention and buffer capacity and the
 2 redistribution of runoff processes by DHF reservoir operation, the T_p of SY and XJWP was higher than that of other regions.



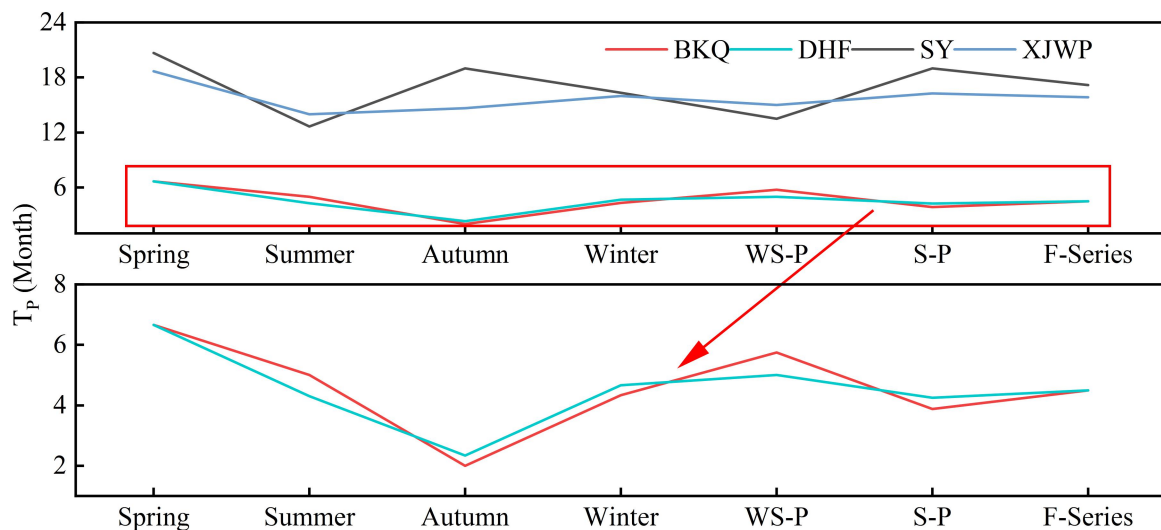
3
 4 **Figure. 8** The correlation between monthly SRI and multi-time scale SPI and the T_p in BKQ (a), DHF (b), SY (c) and XJWP (d).

5 In order to further reveal the changes of T_p , the T_p in different periods are calculated. Fig. 9 expresses the results of the T_p
 6 included the four seasons, water supply period (WS-P), storage period (S-P), and full series (F-series) at the four regions in
 7 the HRB. It is clear from Fig. 9 that, from the point of view of the F-series, the T_p of SY (17.2 months) and XJWP (15.8
 8 months) were obviously higher than the DHF 's (4.5 months), which indicating that the T_p in the area downstream of DHF
 9 Reservoir was significantly postponed. In order to explore the reasons for the postponed of T_p , the evolution of
 10 meteorological factor was explored. The annual precipitation and its variation trend in the control areas of four hydrological
 11 stations during 1967-2019 are shown in Fig. 10. It was clear from Fig. 10 that there was no significant trend in annual
 12 precipitation at four sub-regions during 1967-2019, implying that the prolonged of drought propagation is not due to the
 13 change of meteorological factors. Meanwhile, as Fig. 9 showed, the T_p of BKQ (4.5 months) was equal to DHF 's, whilst
 14 obviously lower than the SY and XJWP 's. Therefore, the construction and operation of DHF reservoir is the main reason for
 15 the significant extension of T_p in the downstream of the reservoir. Many studies have also confirmed the impact of reservoir
 16 operation on hydrological drought (Wu et al., 2016; Wu et al., 2018; Wang et al., 2019). Moreover, the T_p of SY was higher
 17 than the XJWP 's, implying that the improvement effect is weakness with the rising of the interval from hydrological stations
 18 to DHF reservoir.

1 Similar to the F-series, the T_p of SY and XJWP were obviously higher than the BKQ 's in the four seasons, while the T_p of
 2 DHF was not significantly different from that of BKQ. Meanwhile, on the whole, the seasonal variations of T_p in DHF, SY,
 3 and XJWP were brought into line with BKQ with that of BKQ, with long T_p in spring and winter and short in summer and
 4 autumn. Vegetation can consume more water through evapotranspiration during the season with higher temperatures. Higher
 5 temperatures in summer and autumn may be the reason for the relatively long T_p of spring and winter. In addition, there are a
 6 large amount of snow in winter and most of the snow melts in the next spring at HRB. Therefore, the longer T_p in winter and
 7 spring may be caused by the lower temperature in spring and winter and the melting of snow in spring. Besides, it is worth
 8 mentioning that, the T_p of XJWP was longer than that of SY in summer compared to other seasons. This change indicated
 9 that the duration of drought propagation at XJWP in summer was prolonged, which may be due to the partial agricultural
 10 water supply from DHF reservoir directly reaching downstream (XJWP) through channels without passing through SY in
 11 summer.

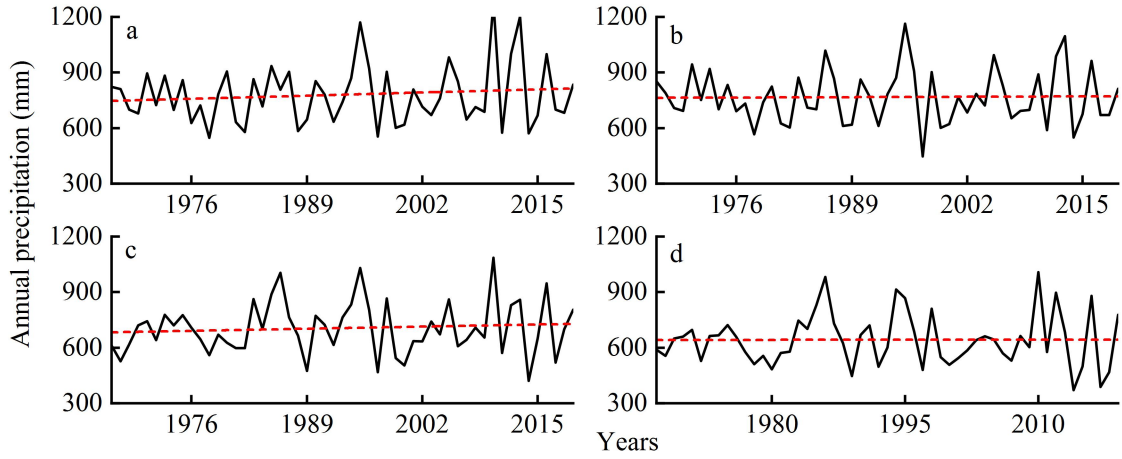
12 For S-P, the T_p of SY and XJWP were both longer than BKQ, and with the rising of interval between hydrological station
 13 and DHF reservoir, the T_p showed a decreasing trend, which showed similar characteristics with the F-series. It is worth
 14 mentioning that the T_p of XJWP is longer than SY during WS-P, which was inconsistent with the conclusion that the T_p
 15 decreases as the increase of the interval between hydrological station and reservoir during S-P. The reason for this is most
 16 likely that part of agricultural water supply from DHF reservoir directly reaching downstream (XJWP) through channels
 17 without passing through SY, which increased runoff at XJWP while SY runoff was little affected. Moreover, agricultural
 18 water supplies mostly occur in the summer, which can be mutually verified with the results of seasonal perspective.

19 In conclusion, the T_p of SY and XJWP were higher than BKQ 's and DHF 's in different periods. The T_p in the
 20 downstream of DHF reservoir has been remarkably strengthened in each period. Moreover, with the rising of interval
 21 between hydrological station and DHF reservoir, the improvement effect was weakened. Meanwhile, the T_p showed longer in
 22 spring and winter, while shorter in summer and autumn and the T_p of XJWP was longer than that of SY in WS-P because of
 23 the effect of agricultural water supply of DHF reservoir.



24

1 **Figure. 9** The T_p of BKQ, DHF, SY and XJWP from meteorological to hydrological drought in different periods.



2
3 **Figure. 10** The variation trend of annual precipitation in the four sub-regions during 1967-2019. (a)-(d) denotes BKQ, DHF, SY and
4 XJWP, respectively.

5 4.4 The drought propagation thresholds for triggering hydrological drought

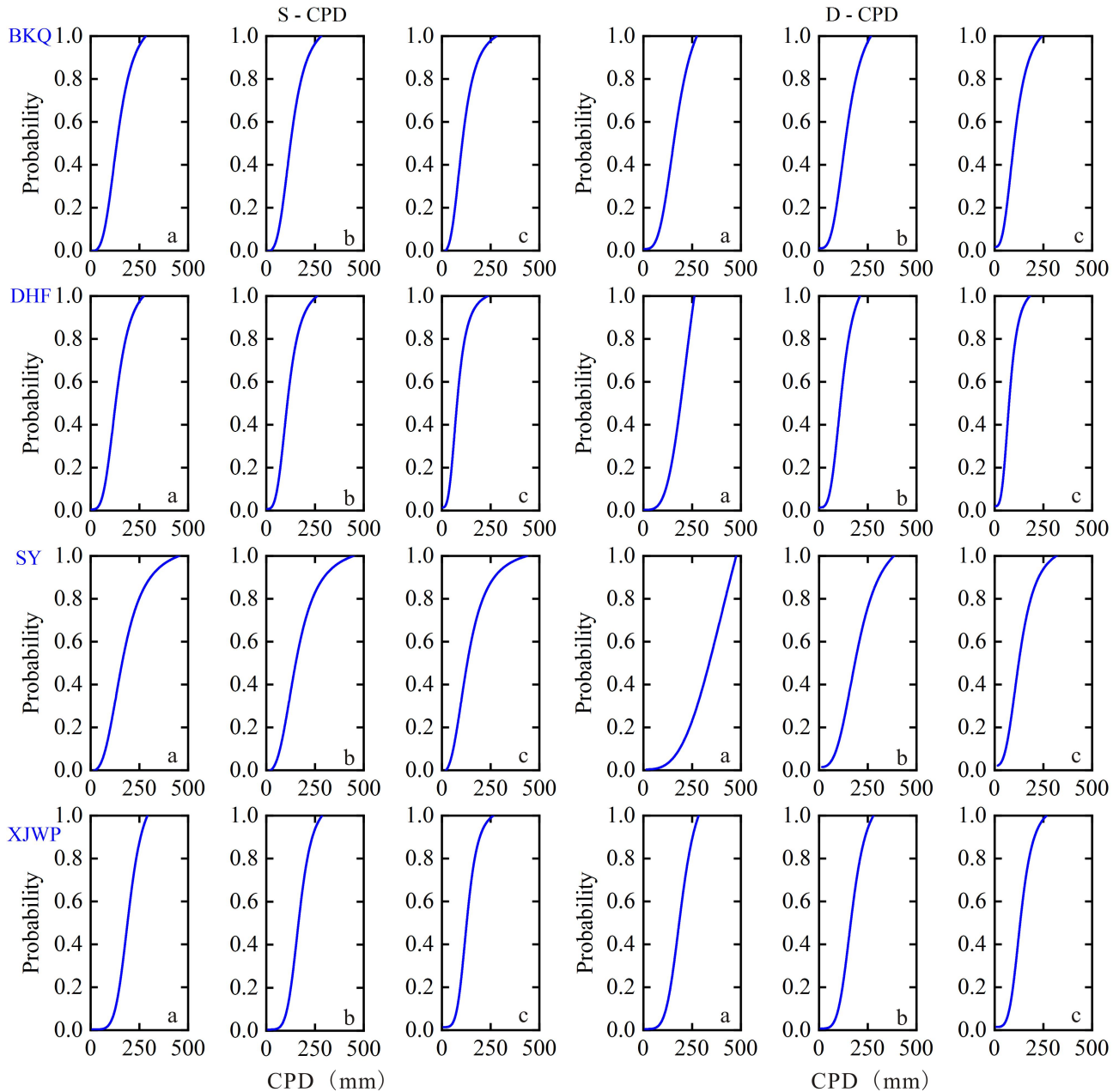
6 In this study, drought propagation threshold model was established to explore the CPD thresholds for triggering hydrological
7 drought. In the model, moderate, severe and extreme hydrological droughts defined in Section 4.2 were selected as specific
8 hydrological drought scenarios. The drought duration and severity of each hydrological drought event were taken as the
9 target respectively, and the corresponding CPD was regarded as the condition. Five common functions including Gamma,
10 EXP, GEV, Logn, and WBL, were used to fit the sequence of CPD in the four sub-basins at HRB. The AIC, RMSE and K-S
11 test were applied to select the best-fit marginal distribution, and the consequences were shown in Table 3. The commonly
12 used bivariate theoretical copula functions, including Clayton, Frank, and Gumbel copula were considered for modeling the
13 dependence structure between CPD and drought duration (D-CPD) and severity (S-CPD), respectively. Based on the K-S,
14 C-M, RMSE and AIC test, the GOF copula functions were selected and shown in Table 6. Fig. 11 shows the conditional
15 probabilities of occurrence different scenarios hydrological droughts characterized by drought duration and severity under
16 the condition of various CPD in four sub-regions. It can be seen from Fig. 11 that the CDP corresponding to the same
17 probability in the four regions increased with the enhancement of drought level. Under the same probability, the CDP of
18 upstream regions (BKQ and DHF) of DHF reservoir is smaller than that of downstream regions (SY and XJWP) with the
19 same level of drought.

20 **Table. 6** GOF evaluation of different copula functions between CPD and drought duration and severity at four sub-regions.

Zones		BKQ		DHF		SY		XJWP	
Copulas	GOF test	D - CPD	S - CPD	D - CPD	S - CPD	D - CPD	S - CPD	D - CPD	S - CPD
	K-S	0.146	0.108	0.108	0.074	0.117	0.102	0.103	0.117
Clayton	C-M	0.099	0.102	0.184	0.053	0.112	0.071	0.075	0.056
	RMSE	0.043	0.044	0.057	0.031	0.055	0.044	0.044	0.038

	AIC	-330.95	-329.45	-324.83	-395.81	-212.48	-229.21	-242.11	-253.53
	K-S	0.110	0.112	0.091	0.054	0.102	0.068	0.107	0.095
Gumbel–Hougaard	C-M	0.092	0.137	0.090	0.037	0.069	0.037	0.077	0.046
	RMSE	0.042	0.051	0.040	0.025	0.043	0.032	0.044	0.034
	AIC	-334.98	-313.61	-365.50	-416.43	-230.42	-267.49	-240.88	-260.96
	K-S	0.120	0.110	0.098	0.048	0.109	0.077	0.105	0.097
Frank	C-M	0.084	0.114	0.108	0.032	0.075	0.047	0.073	0.045
	RMSE	0.040	0.046	0.044	0.024	0.045	0.036	0.043	0.034
	AIC	-339.81	-323.44	-355.05	-424.55	-227.24	-257.85	-243.17	-262.23

1 The bold letters represent the selected optimal copula functions.



2
3 **Figure. 11** Conditional probabilities of occurrence of extreme (a), severe (b), and moderate (c),hydrological drought under
4 the circumstance of various CPD at HRB.

5 In order to quantitatively reveal the threshold triggering different scenarios of hydrological drought, the CPD threshold
6 interval was obtained based on the drought propagation threshold model introduced in Section 3.5 (Table 7). It was clear

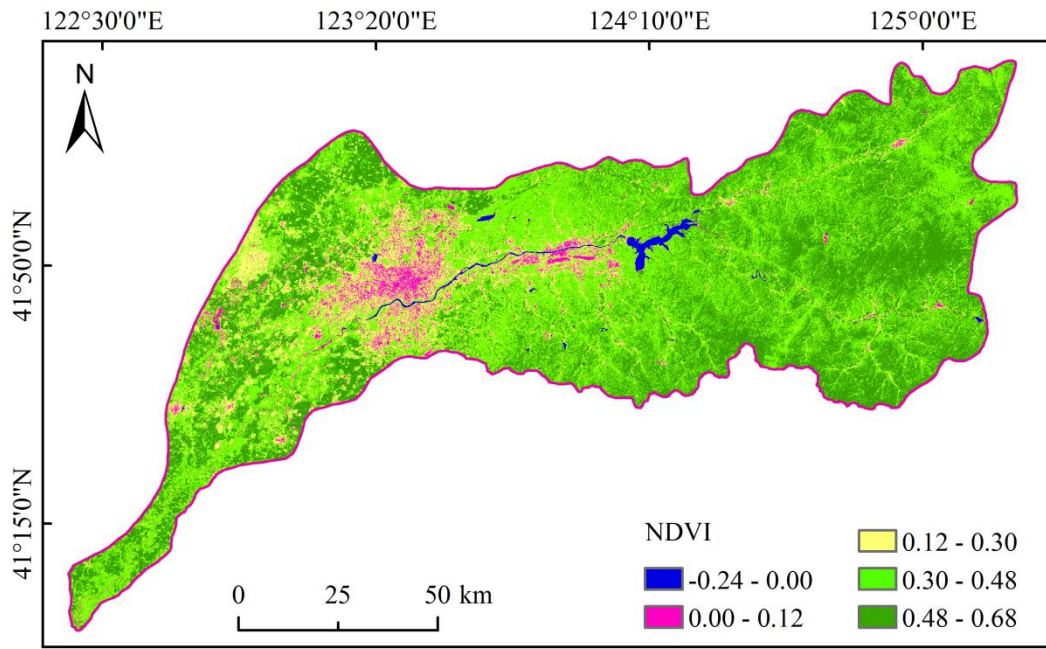
1 from Table 7 that the CPD threshold of hydrological drought at all scenarios in the upstream region (BKQ and DHF) of DHF
2 reservoir are significantly lower than that in the downstream basins (SY and XJWP). The upstream region is located in the
3 eastern part of the HRB with mountainous terrain, while downstream region are in the western plain. The slope of upstream
4 is greater than that of downstream, indicating that the underlying surface of upstream region has less water retention and
5 buffer capacity. Meanwhile, due to the operation of the DHF reservoir, which provides agricultural and ecological water
6 supply to the downstream in May-August, it can provide a strong supply to the downstream and alleviate the hydrological
7 drought (Guo et al., 2020a). Therefore, under the combined action of the the stronger stagnant water and buffer capacity of
8 underlying surface, and the water supply by the operation of DHF reservoir, the CPD threshold in the downstream region of
9 DHF reservoir are significantly higher than that in the upstream basins.

10 For the DHF and BKQ, both of them are located in mountainous areas with higher slope, but the vegetation coverage rate
11 of BKQ is relatively larger than that of DHF, which indicated by the Normalized Difference Vegetation Index (NDVI) of the
12 HRB (Fig. 12). Therefore, BKQ has strong water retention and buffering capacity, which leads to the CDP of BKQ relatively
13 greater than DHF. As for the SY and XJWP, both of them are located in the plain area with little difference in slope.
14 However, the XJWP showed the lower CDP at all scenarios hydrological drought than SY. On the one hand, large reservoirs
15 can postpone the propagation from meteorological drought to hydrological drought, and the effect decreases with the
16 increase of the distance from the reservoir (Guo et al., 2020a). The distance between SY and DHF reservoir is greater than
17 that from XJWP to DHF reservoir. On the other hand, as the urbanization process of SY is much faster than that of XJWP,
18 the vegetation coverage rate of SY is lower than that of XJWP, which was confirmed in Fig. 12. During extreme
19 meteorological droughts, vegetation is in a state of water shortage, and consumes more water through evapotranspiration,
20 which would eaggeravate drought in the basin (Teuling et al., 2013; Niu et al., 2019). Therefore, the higher vegetation
21 coverage in XJWP is another reason why the CDP of the XJWP to extreme drought is lower than the SY.

22 The mean value of CPD thresholds under different drought scenarios and the increase rate (IR) of CPD thresholds as the
23 drought scenario intensified were calculated to investigate the difference of CPD increase rate in each sub-basin with the
24 aggravation of hydrological drought. Table 8 exhibits the mean of CPD thresholds and the IR of CPD under extreme and
25 severe drought relative to moderate drought in each sub-basin. It can be seen from Table 8 that the IR of CPD threshold in
26 BKQ and XJWP were less than that of DHF and SY with the intensifying of drought scenario. Moreover, the IR of CPD
27 threshold from severe drought to extreme drought were much lower than that from moderate drought to severe drought in
28 BKQ and XJWP. These suggest that BKQ and XJWP are more sensitive to CPD in the event of drought, and a slight
29 increase in CPD may trigger a more severe drought. Especially in severe drought scenario, a small increase in CPD is likely
30 to trigger extreme drought. As shown in Fig. 1, DHF and SY are located around DHF reservoir, while BKQ and XJWP are

1 far away from DHF reservoir. Therefore, the cause of this result is most likely to be the operation of DHF reservoir, which
 2 needs further research to confirm.

3 Meanwhile, for a specific hydrological drought, the higher the CPD that triggered this hydrological drought is, the
 4 stronger the drought resistance of this basin is (Guo et al., 2020a). Therefore, the CPD thresholds for triggering hydrological
 5 drought can be employed to characterize the drought resistance of the basin in this study. According to the above CPD
 6 threshold analysis results of sub-basins, the drought resistance of the downstream region of DHF reservoir is stronger than
 7 that of the upstream region under all hydrological drought scenarios. SY showed the strongest resistance for all scenarios
 8 hydrological drought. The difference of drought resistance of each sub-basin mainly depends on the topography of the basin,
 9 the influence of reservoir operation on the watercourse hydraulic conditions and the change of underlying surface conditions
 10 caused by urbanization.



11
 12 **Figure. 12** Normalized Difference Vegetation Index (NDVI) of the HRB.

13 **Table. 7** CPD threshold intervals for triggering different scenarios of hydrological drought at HRB.

Drought scenario		Moderate	Severe	Extreme
BKQ	CPD (mm)	[204.3, 222.4]	[238.2, 239.8]	[246.5, 253.1]
DHF	CPD (mm)	[146.8, 172.5]	[188.7, 213.8]	[234.4, 253.7]
SY	CPD (mm)	[258.0, 321.7]	[339.3, 346.6]	[357.6, 461.7]
XJWP	CPD (mm)	[217.0, 226.3]	[253.8, 255.5]	[265.9, 271.1]

14 **Table. 8** The mean and the IR of CPD thresholds in each sub-basin.

Drought scenario	BKQ		DHF		SY		XJWP	
	CPD (mm)	IR (%)	CPD (mm)	IR (%)	CPD (mm)	IR (%)	CPD (mm)	IR (%)
Extreme	249.8	4.5	244.1	21.3	409.7	19.4	268.5	5.5
Severe	239.0	12.0	201.2	26.1	343.0	18.3	254.6	14.9
Moderate	213.4		159.6		289.9		221.6	

1 5 Conclusions

2 In this paper, SPI and SRI were adopted to characterize meteorological and hydrological drought respectively, and the
3 spatiotemporal variation characteristics of hydrological drought were investigated in the HRB from 1967 to 2019.
4 Meanwhile, the joint distribution of drought duration and intensity was established by using copula function to calculate the
5 return period of hydrological drought. Furthermore, the T_p were determined by calculating the Pearson correlation
6 coefficients between 1-month SRI and multi-time scale SPI. Finally, the CPD threshold intervals for triggering hydrological
7 drought are obtained by the drought propagation threshold model. From the results, primary conclusions are given as
8 follows:

9 (1) Hydrological drought showed a slight strengthening trend in DHF, while presented alternate characteristics of drought
10 and flood in SY and XJWP from 1967 to 2019. From seasonal perspective, drought presented an strengthening trend in each
11 season at DHF. Nevertheless, drought presented an strengthening trend in summer and autumn, while showed a decreasing
12 trend in spring and winter at SY and XJWP.

13 (2) The western and center of the HRB were vulnerable districts to hydrological drought with longer drought duration and
14 higher severity. Furthermore, the eastern region of the HRB was more sensitive to short-duration drought, which was
15 dominated by two-month and three-month drought events.

16 (3) The return periods T_{and} (T_{or}) of moderate, severe, and extreme hydrological drought in DHF, SY and XJWP were 2.3
17 (1.7), 4.5 (3.1), 22.8 (14.9), 3.3 (2.7), 6.7 (4.8), 71.0 (18.6), 3.2 (2.6), 7.3 (4.4) and 79.0 (16.3) years, respectively.

18 (4) The average T_p in BKQ, DHF, SY and XJWP were 4.1, 4.3, 14.9, and 1.9 months, respectively, which indicated that
19 the T_p in the downstream of DHF reservoir has been significantly improved owing to the operation of DHF. Moreover, with
20 the increase of interval between hydrological station and DHF reservoir, the improvement effect was weakened.

21 (5) The mean CPD thresholds of moderate hydrological drought at BKQ, DHF, SY and XJWP were 213.4, 159.6, 289.9
22 and 221.6 mm, severe were 239.0, 201.2, 343.0 and 254.6 mm, and extreme were 249.8, 244.1, 409.7 and 268.5 mm,
23 respectively. And, the difference of CPD thresholds of each sub-basin mainly depends on the topography of the basin, the
24 evolution of river hydraulic condition by reservoir operation and the change of underlying surface conditions caused by
25 urbanization.

26 **Data availability.** Some or all data, models, or code that support the findings of this study are available from the
27 corresponding author upon reasonable request.

28
29 **Author Contribution.** Conceptualization: S P.Y.; F T.Y. Methodology: F T.Y.; S P.Y.; X D.S. Data
30 gather: X D.S.; S P.Y. Formal analysis and investigation: S P.Y.; X D.S.; F T.Y. Writing
31 manuscript: S P.Y.; F T.Y.

1 **Conflicts of interest.** The authors declare that they have no known competing financial interests or personal relationships
2 that could have appeared to influence the work reported in this paper.

3

4 **References**

- 5 ■ Barker, L. J., Hannaford, J., Chiverton, A., and Svensson, C.: From meteorological to hydrological drought using
6 standardised indicators, *Hydrol. Earth Syst. Sci.*, 20, 2483–2505, <https://doi.org/10.5194/hess-20-2483-2016>, 2016.
- 7 ■ Beniston, M., and Stephenson, D.B.: Extreme climatic events and their evolution under changing climatic conditions,
8 *Glob. Planet. Change.*, 44, 1-9, <https://doi.org/10.1016/j.gloplacha.2004.06.001>, 2004.
- 9 ■ Chang, J., Guo, A., Wang, Y., Ha, Y., Zhang, R., Xue, L., and Tu, Z.: Reservoir operations to mitigate drought effects
10 with a hedging policy triggered by the drought prevention limiting water level, *Water Resour. Res.*, 55, 904-922,
11 <https://doi.org/10.1029/2017WR022090>, 2019.
- 12 ■ Chen, X., Li, F.W., and Feng, P.: Spatiotemporal variation of hydrological drought based on the Optimal Standardized
13 Streamflow Index in Luanhe River basin, China, *Nat. Hazards.*, 91, 155-178,
14 <https://doi.org/10.1007/s11069-017-3118-6>, 2018.
- 15 ■ Christensen, O.B., and Christensen, J.H.: Intensification of extreme European summer precipitation in a warmer climate,
16 *Global Planet. Change.*, 44, 107-117, <https://doi.org/10.1016/j.gloplacha.2004.06.013>, 2004.
- 17 ■ Dash, S.S., Sahoo, B., and Raghuwanshi, N.S.: A SWAT-Copula based approach for monitoring and assessment of
18 drought propagation in an irrigation command, *Ecol. Eng.*, 127, 417- 430,
19 <https://doi.org/10.1016/j.ecoleng.2018.11.021>, 2019.
- 20 ■ Fang, W., Huang, S., Huang, Q., Huang, G., Wang, H., Leng, G., Wang, L., and Guo, Y.: Probabilistic assessment of
21 remote sensing-based terrestrial vegetation vulnerability to drought stress of the Loess Plateau in China, *Remote Sens.*
22 *Environ.*, 232, 111292, <https://doi.org/10.1016/j.rse.2019.111290>, 2019.
- 23 ■ Genest, C., Kojadinovic, I., Nešlehová, J., and Yan, j.: A goodness-of-fit test for bivariate extreme-value copulas,
24 *Bernoulli.*, 17 (1) 253 - 275, <https://doi.org/10.3150/10-BEJ279>, 2011.
- 25 ■ Gevaert, A.I., Veldkamp, T.I.E., and Ward, P.J.: The effect of climate type on timescales of drought propagation in an
26 ensemble of global hydrological models, *Hydrol. Earth Syst. Sci.*, 22, 4649-4665,
27 <https://doi.org/10.5194/hess-22-4649-2018>, 2018.
- 28 ■ Guo, Y., Huang, Q., Huang, S.Z., Leng, G.Y., Zheng, X.D., Fang, W., Deng, M.J., Song, S.B.: Elucidating the effects
29 of mega reservoir on watershed drought tolerance based on a drought propagation analytical method, *J. Hydrol.*, 598,
30 125738, <https://doi.org/10.1016/j.jhydrol.2020.125738>, 2020a.

- 1 ■ Guo, Y., Huang, S.Z., Huang, Q., Leng, G.Y., Fang, W., Wang, L., and Wang, H.: Propagation thresholds of
2 meteorological drought for triggering hydrological drought at various levels, *Science of The Total Environment.*, 712,
3 136502, <https://doi.org/10.1016/j.scitotenv.2020.136502>, 2020b.
- 4 ■ Guo, Y., Huang, S.Z., Huang, Q., Wang, H., Fang, W., Yang, Y.Y., and Wang, L.: Assessing socioeconomic drought
5 based on an improved multivariate standardized reliability and resilience index, *J. Hydrol.*, 568, 904-918,
6 <https://doi.org/10.1016/j.jhydrol.2018.11.055>, 2019.
- 7 ■ Huang, S., Li, P., Huang, Q., Leng, G., Hou, B., Ma, L.: The propagation from meteorological to hydrological drought
8 and its potential influence factors, *J. Hydrol.*, 547, 184–195, <https://doi.org/10.1016/j.jhydrol.2017.01.041>, 2017.
- 9 ■ Huang, S.Z., Chang, J.X., Leng, G.Y., and Huang, Q.: Integrated index for drought assessment based on variable fuzzy
10 set theory: a case study in the Yellow River basin, China, *J. Hydrol.*, 527, 608-618,
11 <https://doi.org/10.1016/j.jhydrol.2015.05.032>, 2015.
- 12 ■ Huang, W.C., and Chou, C.C.: Risk-based drought early warning system in reservoir operation, *Adv. Water Resour.*, 31,
13 649-660, <https://doi.org/10.1016/j.advwatres.2007.12.004>, 2008.
- 14 ■ Joetzer, E., Douville, H., Delire, C., Ciais, P., Decharme, B., and Tyteca, S.: Hydrologic benchmarking of
15 meteorological drought indices at interannual to climate change timescales: a case study over the Amazon and
16 Mississippi river basins, *Hydrol. Earth Syst. Sci.*, 17, 4885–4895, <https://doi.org/10.5194/hess-17-4885-2013>, 2013.
- 17 ■ Kao, S.C., and Govindaraju, R.S.: A copula-based joint deficit index for droughts, *J. Hydrol.*, 380 (1-2), 121-134,
18 <https://doi.org/10.1016/j.jhydrol.2009.10.029>, 2009.
- 19 ■ Kendall, M.G.: *Rank Correlation Methods*. Griffin, London, 1975.
- 20 ■ Kim, S., Kim, B., Ahn, T.J., and Kim, H.S.: Spatio-temporal characterization of Korean drought using
21 severity-area-duration curve analysis, *Water Environ. J.*, 25 (1), 22-30,
22 <https://doi.org/10.1111/j.1747-6593.2009.00184.x>, 2011.
- 23 ■ Kunkel, K.E.: North American trends in extreme precipitation, *Nat. Hazards.*, 29, 291-305,
24 <https://doi.org/10.1023/A:1023694115864>, 2003.
- 25 ■ Lee, T., Modarres, R., and Ouarda, T.B.M.J.: Data-based analysis of bivariate copula tail dependence for drought
26 duration and severity, *Hydrol. Processes.*, 27, 1454-1463, <https://doi.org/10.1002/hyp.9233>, 2013.
- 27 ■ Leng, G.Y., Tang, Q.H., and Rayburg, S.: Climate change impacts on meteorological, agricultural and hydrological
28 droughts in China, *Global Planet. Change.*, 126, 23-34, <https://doi.org/10.1016/j.gloplacha.2015.01.003>, 2015.
- 29 ■ Lindenschmidt, K.E., and Rokaya, P.: A stochastic hydraulic modelling approach to determining the probable
30 maximum staging of Ice-Jam floods, *J. Environ. Informatics.*, 34 (1), 45-54, <https://doi.org/10.3808/jei.201900416>,
31 2019.

- 1 ■ Liu, Z.P., Wang, Y.Q., Shao, M.G., Jia, X.X., and Li, X.L.: Spatiotemporal analysis of multiscalar drought
2 characteristics across the Loess Plateau of China, *J. Hydrol.*, 534, 281-299,
3 <https://doi.org/10.1016/j.jhydrol.2016.01.003>, 2016a.
- 4 ■ Liu, Z.Y., Menzel, L., Dong, C.Y., and Fang, R.H.: Temporal dynamics and spatial patterns of drought and the relation
5 to ENSO: A case study in Northwest China, *Int. J. Climatol.*, 36 (8), 2886-2898, <https://doi.org/10.1002/joc.4526>,
6 2016b.
- 7 ■ Lorenzo-Lacruz, J., Vicente-Serrano, S.M., González-Hidalgo, J.C., López-Moreno, J.I., and Cortesi, N.: Hydrological
8 drought response to meteorological drought in the Iberian Peninsula, *Clim. Res.*, 58, 117-131,
9 <https://www.jstor.org/stable/24896134>, 2013.
- 10 ■ Mann, H.B.: Nonparametric tests against trend, *Econometrica.*, 13 (3), 245–259, <https://doi.org/10.2307/1907187>, 1945.
- 11 ■ McKee, T.B.N., Doesken, J., and Kleist, J.: The relationship of drought frequency and duration to time scales, In: Eight
12 Conf. On Applied Climatology, Anaheim, CA, Amer. Meteor. Soc., pp, 179-184, 1993.
- 13 ■ Mirabbasi, R., Fakheri-Fard, A., and Dinpashoh, Y.: Bivariate drought frequency analysis using the copula method,
14 *Theor. Appl. Climatol.*, 108 (1-2), 191-206, <https://doi.org/10.1007/s00704-011-0524-7>, 2012.
- 15 ■ Mishra, A.K., and Singh, V.P.: Drought modelling – a review. *J. Hydrol.*, 403, 157-175,
16 <https://doi.org/10.1016/j.jhydrol.2011.03.049>, 2011.
- 17 ■ Mishra, A.K., Singh, V.P.: A review of drought concepts, *J. Hydrol.*, 391, 202–216,
18 <https://doi.org/10.1016/j.jhydrol.2010.07.012>, 2010.
- 19 ■ Niu, Z., He, H., Zhu, G., Ren, X., Zhang, L., Zhang, K., Yu, G., Ge, R., Li, P., Zeng, N., Zhu, X.: An increasing trend
20 in the ratio of transpiration to total terrestrial evapotranspiration in China from 1982 to 2015 caused by greening and
21 warming. *Agric. For. Meteorol.*, 279, 107701, <https://doi.org/10.1016/j.agrformet.2019.107701>, 2019.
- 22 ■ Oladipo, E.O.: A comparative performance analysis of three meteorological drought indices, *J. Clim.*, 5, 655–664,
23 <https://doi.org/10.1002/joc.3370050607>, 1985.
- 24 ■ Palmer, T.N., and Räisänen, J.: Quantifying the risk of extreme seasonal precipitation events in a changing climate,
25 *Nature.*, 415, 512-514, <https://doi.org/10.1038/415512a>, 2002.
- 26 ■ Pandey, R.P., and Ramasastri, K.S.: Relationship between the common climatic parameters and average drought
27 frequency, *Hydrol. Processes.*, 15, 1019-1032, <https://doi.org/10.1002/hyp.187>, 2001.
- 28 ■ Rad, A.M., Ghahraman, B., Khalili, D., Ghahremani, Z., and Ardakani, S.A.: Integrated meteorological and
29 hydrological drought model: A management tool for proactive water resources planning of semi-arid regions, *Advances*
30 *in Water Resources.*, 107, 336-353, <https://doi.org/10.1016/j.advwatres.2017.07.007>, 2017.

- 1 ■ Rivera, J.A., Penalba, O.C., Villalba, R., and Araneo, D.C.: Spatio-temporal patterns of the 2010-2015 extreme
2 hydrological drought across the Central Andes, Argentina, *Water.*, 9, 652, <https://doi.org/10.3390/w9090652>, 2017.
- 3 ■ Sattar, M.N., Lee, J.Y., Shin, J.Y., and Kim, T.W.: Probabilistic characteristics of drought propagation from
4 meteorological to hydrological drought in South Korea, *Water Resour. Manag.*, 33, 2439-2452,
5 <https://doi.org/10.1007/s11269-019-02278-9>, 2019.
- 6 ■ Shiklomanov, I.A., Shiklomanov, A.I., Lammers, R.B., Peterson, B.J., and Vorosmarty, C.J.: The dynamics of river
7 water inflow to the arctic ocean, *Freshw. Budget Arctic Ocean.*, 281-296,
8 https://doi.org/10.1007/978-94-011-4132-1_13, 2000.
- 9 ■ Shukla, S. and Wood, A.W.: Use of a standardized runoff index for characterizing hydrologic drought, *Geophys. Res.*
10 *Lett.*, 35, 41–46, <https://doi.org/10.1029/2007GL032487>, 2008.
- 11 ■ Sun, S.L., Li, Q., Li, J., and Wang, G.: Revisiting the evolution of the 2009-2011 meteorological drought over
12 Southwest China, *J. Hydrol.*, 568, 385-402, <https://doi.org/10.1016/j.jhydrol.2018.10.071>, 2019.
- 13 ■ Teuling, A.J., Van Loon, A.F., Seneviratne, S.I., Lehner, I., Aubinet, M., Heinesch, B., Bernhofer, C., Grünwald, T.,
14 Prasse, H., Spank, U.: Evapotranspiration amplifies European summer drought. *Geophys. Res. Lett.*, 40, 2071–2075,
15 <https://doi.org/10.1002/grl.50495>, 2013.
- 16 ■ Van Lanen, H. A. J., Wanders, N., Tallaksen, L. M., and Van Loon, A. F.: Hydrological drought across the world:
17 impact of climate and physical catchment structure, *Hydrol. Earth Syst. Sci.*, 17, 1715–1732,
18 <https://doi.org/10.5194/hess-17-1715-2013>, 2013.
- 19 ■ Van Loon, A.F., Van Huijgevoort, M.H.J., and Van Lanen, H.A.J.: Evaluation of drought propagation in an ensemble
20 mean of large-scale hydrological models, *Hydrol. Earth Syst. Sci.*, 16, 4057-4078,
21 <https://doi.org/10.5194/hess-16-4057-2012>, 2012.
- 22 ■ Vicente-Serrano, S. M. and López-Moreno, J. I.: Hydrological response to different time scales of climatological
23 drought: an evaluation of the Standardized Precipitation Index in a mountainous Mediterranean basin, *Hydrol. Earth*
24 *Syst. Sci.*, 9, 523–533, <https://doi.org/10.5194/hess-9-523-2005>, 2005.
- 25 ■ Vicente-Serrano, S.M., López-Moreno, J.I., Beguería, S., Lorenzo-Lacruz, J., AzorinMolina, C., and Morán-Tejeda, E.:
26 Accurate computation of a streamflow drought index, *J. Hydrol. Eng.*, 17, 318-332,
27 [https://doi.org/10.1061/\(ASCE\)HE.1943-5584.0000433](https://doi.org/10.1061/(ASCE)HE.1943-5584.0000433), 2012.
- 28 ■ Vyver, H.V.D., and Bergh, J.V.D.: The Gaussian copula model for the joint deficit index for droughts, *J. Hydrol.*, 561,
29 987-999, <https://doi.org/10.1016/j.jhydrol.2018.03.064>, 2018.

- 1 ■ Wang, F., Wang, Z.M., Yang, H.B., Di, D.Y., Zhao, Y., Liang, Q.H., and Hussain, Z.: Comprehensive evaluation of
2 hydrological drought and its relationships with meteorological drought in the Yellow River basin, China, *J. Hydrol.*,
3 584, 124751, <https://doi.org/10.1016/j.jhydrol.2020.124751>, 2020.
- 4 ■ Wang, Y.M., Yang, J., Chang, J.X., and Zhang, R.: Assessing the drought mitigation ability of the reservoir in the
5 downstream of the Yellow River, *Sci. Total Environ.*, 646, 1327-1335, <https://doi.org/10.1016/j.scitotenv.2018.07.316>,
6 2019.
- 7 ■ Wilhite, D.A., and Glantz, M.H.: Understanding: the drought phenomenon: the role of definitions, *Water Int.*, 10,
8 111-120, <https://doi.org/10.1080/02508068508686328>, 1985.
- 9 ■ Wu, J.F., Chen, X.W., Gao, L., Yao, H.X., Chen, Y., Liu, and M.B., Shukla, S.: Response of hydrological drought to
10 meteorological drought under the influence of large reservoir, *Adv. Meteorol.*, 2016, 1-11,
11 <https://doi.org/10.1155/2016/2197142>, 2016.
- 12 ■ Wu, J.F., Chen, X.W., Yao, H.X., Gao, L., Chen, Y., and Liu, M.B.: Non-linear relationship of hydrological drought
13 responding to meteorological drought and impact of a large reservoir, *J. Hydrol.*, 551, 495-507,
14 <https://doi.org/10.1016/j.jhydrol.2017.06.029>, 2017.
- 15 ■ Wu, J.F., Liu, Z.Y., Yao, H.X., Chen, X.H, Chen, X.W, Zheng, Y.H., and He, Y.H.: Impacts of reservoir operations on
16 multi-scale correlations between hydrological drought and meteorological drought, *J. Hydrol.*, 563, 726-736,
17 <https://doi.org/10.1016/j.jhydrol.2018.06.053>, 2018.
- 18 ■ Xu, K., Yang, D.W., Xu, X.Y., and Lei, H.M.: Copula based drought frequency analysis considering the
19 spatio-temporal variability in Southwest China, *J. Hydrol.*, 527, 630-640, <https://doi.org/10.1016/j.jhydrol.2015.05.030>,
20 2015.
- 21 ■ Xu, Y., Zhang, X., Wang, X., Hao, Z.C., Singh, V.P., and Hao, F.H.: Propagation from meteorological drought to
22 hydrological drought under the impact of human activities: a case study in northern China, *J. Hydrol.*, 579, 124147,
23 <https://doi.org/10.1016/j.jhydrol.2019.124147>, 2019.
- 24 ■ Yang, X., Li, Y.P., Liu, Y.R., and Gao, P.P.: A MCMC-based maximum entropy copula method for bivariate drought
25 risk analysis of the Amu Darya River Basin, *J. Hydrol.*, 590, 125502, <https://doi.org/10.1016/j.jhydrol.2020.125502>,
26 2020.
- 27 ■ Yevjevich, V.: An objective approach to definitions and investigations of continental hydrologic droughts: Vujica
28 Yevjevich: Fort Collins, Colorado State University, 1967, 19 p. (Hydrology paper no. 23),
29 [https://doi.org/10.1016/0022-1694\(69\)90110-3](https://doi.org/10.1016/0022-1694(69)90110-3), 1967.

- 1 ■ Zhao, P.P., Lu, H.S., Fu, G.B., Zhu, Y.H., Su, J.B., and Wang, J.Q.: Uncertainty of hydrological drought characteristics
- 2 with copula functions and probability distributions: a case study of Weihe River, China, *Water*, 9 (5), 334,
- 3 <https://doi.org/10.3390/w9050334>, 2017.